CLOSED MAGNETIC STRUCTURES IN THE CHROMOSPHERE AND IN THE TRANSITION REGION

J. M. MALHERBE, B. SCHMIEDER, G. SIMON, P. MEIN,
Observatoire de Paris, Section de Meudon, 92195 Meudon Principal Cedex, France

and

E. TANDBERG-HANSSEN
NASA, Marshall Space Flight Center, AL 35812, U.S.A.

(Received 3 June, 1986; in revised form 29 June, 1987)

Abstract. Using simultaneous observations of the same solar regions in the lines Hα and C IV 1548 Å, we have derived schematic models of closed magnetic lines from dynamical constraints. We conclude that the magnetic loops are closed at higher levels above facular than above non-facular regions. This result remains valid whatever are the assumed density models and even if we take into account the 3 min oscillations. The center-to-limb behaviour is well predicted by taking into account the relative opacity in chromosphere and transition region.

1. Introduction

In the past few years there has been substantial progress in the understanding of the mass and energy flow in the outer solar atmosphere (Withbroe and Noyes, 1977). Ground-based (Mein *et al.*, 1982) and space observations (Athay and White, 1978) have pointed out that the mechanical flux in the high levels of the solar atmosphere is much smaller than previously indicated using the energy conservation law. The reflection of waves in the high chromosphere could explain this discrepancy (Mein and Provost, 1979). The velocity field in the transition region has been extensively studied by space instruments. According to different authors, a predominant redshift is evidenced from 5 to 12 km s^{-1} referring to cool lines (Doschek *et al.*, 1976; Roussel-Dupré and Shine, 1982; Brueckner, 1981) or using averaged velocity value over a large solar area (Gebbie *et al.*, 1981). Their properties has been studied such as the dependence of C IV Doppler shifts on solar latitude (Dere *et al.*, 1982), the association of relative downflow and regon of network emission (Gebbie *et al.*, 1981). Only few studies compare velocity fields between the chromosphere and the transition region because required coordinated ground based and space observations are scarce.

Among the above mentioned comparison studies, some consider the velocity field observed in and around filaments (Schmieder *et al.*, 1984a), while others deal with the velocity over larger areas (Mein *et al.*, 1982). The last authors find a flux ratio between the transition region and the chromosphere smaller by a factor of 7 compared to the value expected from usual chromospheric density models. They interpret this result as the effect of the curvature of magnetic field lines anchored in faculae. This argues in

Solar Physics **112** (1987) 233–253.

favour of the existence of canopies in the chromosphere, horizontal magnetic field line structures as described by Jones and Giovanelli (1982). Giovanelli and Jones (1982) found that the canopy base lies near the temperature minimum, i.e., roughly five scale heights below commonly accepted values. The canopy height depends on the strength of magnetic field about 150–200 km in the penumbra, 500 to 700 km in areas surrounding active regions. The magnetic field lines connecting high magnetic field regions to neighbouring regions, present an obvious curvature. In order to explore such geometry in the chromosphere, observations at different locations on the disk and at different levels in the atmosphere are necessary.

The observations made with the UVSP spectrometer on the SMM satellite and with the MSDP spectrograph operating in the Meudon Solar Tower provide an opportunity to study the dynamic behaviour of the atmosphere, observed simultaneously in the Hα and C IV lines and located at different solar distances from the center of the disk. We present statistical results relative to the velocity field and the velocity standard deviation measured in the chromosphere and in the transition region, concerning two different kinds of regions: in and outside faculae. We discuss the results according to the density models and propose geometrical structures of the magnetic field for both regions.

2. Observations

2.1. INSTRUMENTATIONS

The Multichannel Subtractive Double Pass (MSDP) spectrograph of the Meudon Solar Tower provides two dimensional observations of Hα Doppler shifts and intensities in the same region. The MSDP instrument and data processing are described by Mein (1977). The total field of view is $5' \times 8'$ with a typical spatial resolution of $1''$. The calibration of the velocity is determined by assuming that the mean Doppler velocity over selected regions is zero. (The selection is such that high velocity patterns are avoided.)

The Ultraviolet Spectrometer and Polarimeter (UVSP) on board the Solar Maximum Mission satellite performed at the same time Dopplergrams in the 1548 Å C IV resonance line (Woodgate *et al.*, 1980). Velocity and intensity maps were obtained in a field $4' \times 4'$ with a spatial resolution $3'' \times 3''$. Velocities were derived from the intensities recorded by two detectors in a bandwidth of 0.3 Å, located approximately at ± 0.15 Å from line center. The total field was scanned in 8 to 10 min. It is assumed that the line Doppler width is 0.15 Å at any pixel and that the mean velocity is nul over the whole field of view. An estimation of the uncertainties has been made by Gebbie *et al.* (1981) and Simon *et al.* (1982): the error in relative velocity is less than 3 km s^{-1} for most of the pixels. Absolute velocity errors may be larger, however, since the previously cited observations (see Introduction) indicate a mean absolute red shift of 5–12 km s^{-1}.

In order to derive the most valuable correlations, UVSP fields were compared to the ground based pictures obtained during the scan. The facular areas were delimited by using Meudon or Marshall magnetograms. We take into account only faculae super-

posed on areas with magnetic field greater than 150–200 G (Table II). At the limb no magnetogram data exist and we define the faculae by high brightness.

2.2. Selected observations

We selected days of observations during the solar maximum year 1980 corresponding to six different distances from the disk center, $r = \sin\theta$, θ being the angle between the line-of-sight and the local vertical (Table I, column 2).

TABLE I

Observational data corresponding to the whole field of view in the Hα and C IV (<4′ × 4′)

	r	UVSP		MSDP UT	σ_V km s^{-1}		$\mathscr{C}$		$\frac{\sigma_{V_{C\,IV}}}{\sigma_{V_{H\alpha}}}$
		Orbit No.	UT		C IV	Hα	$\frac{I_{H\alpha}}{I_{C\,IV}}$	$\frac{V_{H\alpha}}{V_{C\,IV}}$	
(1)	(2)	(3)	(4)	(5)	(6)	(7)	(8)	(9)	(10)
1 Sept., 1980	0.26	11033	12:32	12:33:30	8.21	0.91	0.205	0.218	9.4
		11036	14:08						
11 Sept., 1980	0.29	11412	15:20	14:53:20	8.1	0.80	0.15	0.16	9.8
2 Oct., 1980	0.35	12675	8:13		7.15				
		12681	9:52	9:57	7.2	0.94	0.365	0.237	7.2
		12687	11:28	11:35:20	7.2	1.07	0.479	0.400	
		12693	12:46		7.56				
		12700	14:22		7.01				
28 Sept., 1980	0.5	12464	14:34	14:35:30	9.10	0.95	0.423	0.312	9.4
		12471	16:10	16:18:16	8.4	0.949	0.454	0.367	
9 Oct., 1980	0.5	13194	10:53		7.80				
		13201	12:28		8.35				
		13208	14:04	14:10:22	8.5	1.06	0.405	0.35	8.1
1 May, 1980	0.84	2239	7:10	1:17:20	8.48	1.32	0.356	0.2	
		2241	7:21		8.60				6.87
		2243	7:31		8.96				
		2255	10:30		9.29				
		2257	10:41		9.07				
		2265	12:19		9.79				
		2267	12:30		8.95				
26 Sept., 1980	0.9	12301	14:41	14:31:34	8.10	1.57	0.2		5.16
Days	6r	21 obs.		9 obs.	8.30		0.350	0.280	

The observations in Hα and in C IV were matched as well as the spatial resolution of C IV allowed in both lines. Coefficient of correlation between the intensities and between the velocities were calculated. Generally the velocity correlation value (~ 0.280) is lower than the intensity value (~ 0.350) (Table I, columns 8 and 9).

These coefficients are also lower than those calculated for particular magnetic structures such as filaments, i.e., 0.5 (Schmieder *et al.*, 1984a). If we compare intensity maps in C IV and Hα, most of the faculae and the filaments observed in the Hα line correspond

to bright and dark structures in the C IV line, but this is not always the case: in particular, bright points in C IV do not correspond to any bright feature in Hα (1 September, 1980) which suggests the presence of a hot loop, the top visible only in C IV. Generally downflows in Hα and C IV are well correlated and correspond to bright regions. The velocity correlation value in facular fields reaches 0.6 (Table II, column 5). This confirms previous results (Mein *et al.*, 1981). Upflows are observed principally in filament regions, in good agreement with results obtained by Malherbe *et al.* (1983) and Schmieder *et al.* (1984a).

TABLE II

Facula characteristics

	r	Magneto-grams from	B	$\mathscr{C}$ $V_{H\alpha}/V_{C\,IV}$	σ_V km s^{-1}		$\sigma_{V_{C\,IV}}/\sigma_{V_{H\alpha}}$
					Hα	C IV	
(1)	(2)	(3)	(4)	(5)	(6)	(7)	(8)
1 Sept., 1980	0.26	Marshall		0.506	0.87 1.05 } 1.2 1.7	9.74 7.8 } 8.77	7.3
20 Oct., 1980	0.35	Meudon	200	0.342	1.0 1.1	5.6	
			500	0.362	1.7 } 1.4	} 6.2	4.5
					0.91	4.3	
			500	0.33	2.3	8.7	
9 Oct., 1980	0.5	Meudon	150	0.442	1.7	7.85	
			150	0.447	2.0 } 1.86	7.05 } 7.9	4.2
			150	0.620	1.9	8.89	
1 May, 1980	0.84			0.377	2.8	8	2.8

The hypothesis of null mean velocity over the field of view in our observations may contradict other authors (Gebbie *et al.*, 1981; Roussel-Dupré and Shine, 1982; Athay *et al.*, 1983; Mariska, 1986) who measured a mean steady downflow of 4 to 12 km s^{-1} in the transition region. Nevertheless, it must be noted that these measurements give a strong weight to bright facular regions. In our case, the zero velocity level has been determined by averaging the Doppler velocity over the whole field of view, where the area of non-facular region is quite large.

We present in Figure 1 fields of view corresponding to two different locations (r = 0.5, θ = 30° on 9 October, 1980 and r = 0.84, θ = 60° on 1 May, 1980). In Figure 2 are represented the contours of the Doppler shifts measured in Hα ± 0.3 Å and in C IV for the same regions as mentioned in Figure 1. The boxes indicate the facula areas selected. The observations for the other dates are already published in studies of filaments or surges (Schmieder *et al.*, 1984a, b).

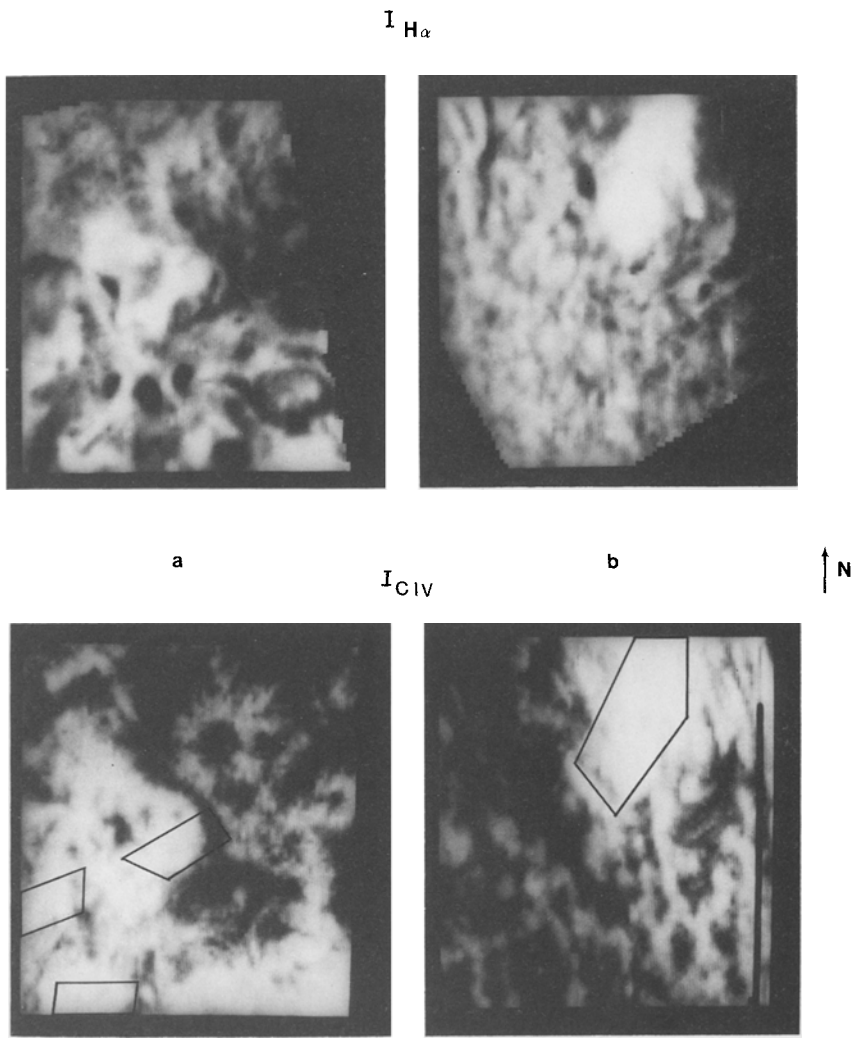

Fig. 1. Intensity maps in the Hα and C IV lines of 4′ × 4′ observed regions. (a) 9 October, 1980 (disk center), (b) 1 May, 1980 (near the limb). White regions are the bright ones. The boxes indicate the location of the studied faculae.

3. Center to Limb Variation of the Velocities

3.1. Statistical analysis

For each pair of observations (in the C IV and Hα lines) we calculated the histogram between Hα and C IV Doppler shifts, $V_{H\alpha}$ and $V_{C\,IV}$, and the mean functions $\overline{V}_{C\,IV}(V_{H\alpha})$:

$$\overline{V}_{C\,IV}(V_{H\alpha}) = \frac{1}{m}\sum_{i=1}^{m} V_{i\,C\,IV}(V_{H\alpha}),$$

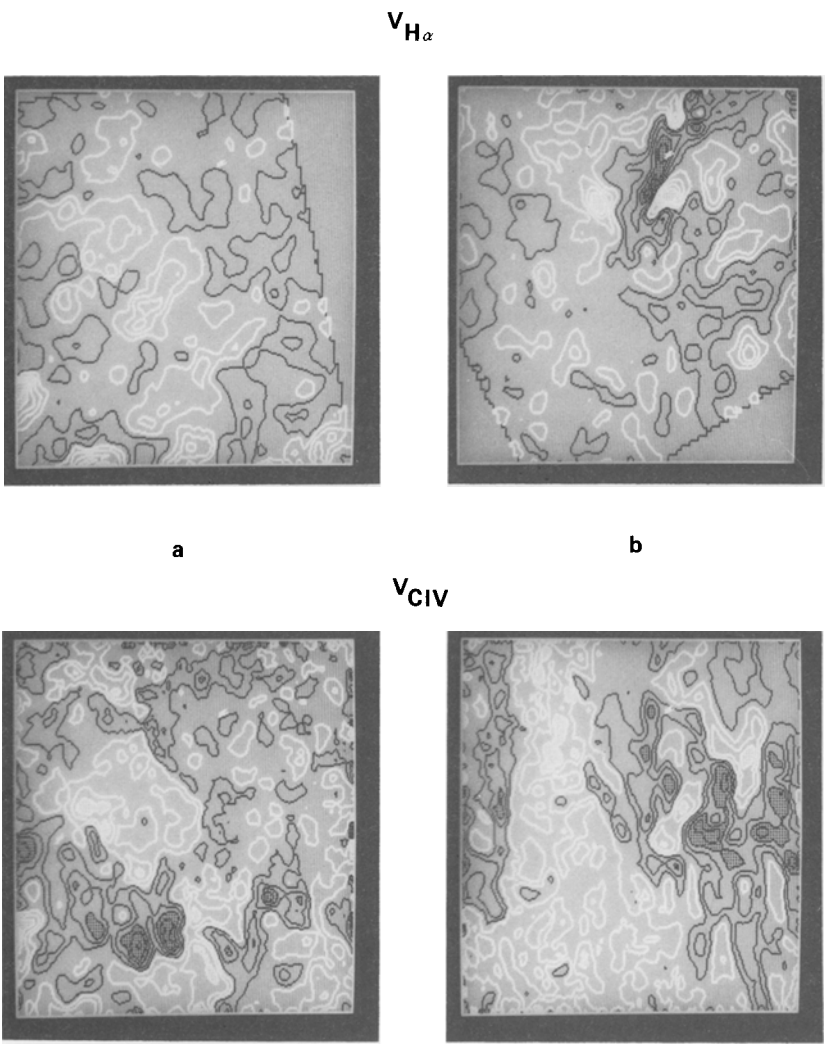

Fig. 2. Velocity maps in the Hα and C IV lines: (a) 9 October, 1980, (b) 1 May, 1980. White contours: red shift; black contours: blue shift; $V_{H\alpha} = \pm 0.5, 1.5, 2.5$ km s^{-1}; $V_{C\,IV} = \pm 2.5, 7.5, 12.5$ km s^{-1}.

which is the averaged value of the C IV velocities corresponding to the m solar points having an Hα velocity equal to $V_{H\alpha}$.

For each observation the velocity standard deviation was obtained as

$$\sigma_{V_\lambda}(r) = \frac{1}{t}\sqrt{t\sum_{i=1}^{t}(V_{i\lambda}(r))^2 - (\sum_{i=1}^{t} V_{i\lambda}(r))^2},$$

where r is the distance to the disk center, λ the wavelength of the line (C IV or Hα), and t the total number of points of the maps. We notice that the mean value $V_{i\lambda}(r)$ is equal

to zero generally according to the zero definition assumed for the velocities, this leads to $\sigma_{V\lambda}(r) \approx$ r.m.s. $(V_\lambda(r))$. The results are presented in Tables I and II.

3.2. Histograms of $V_{C\,IV}/V_{H\alpha}$

Figure 3 shows histograms between C IV and Hα velocity calculated in the same active region:

(1) The region is located near disk center (2 October, 1980). The positive Hα Doppler shift values are lower than the negative ones. This means that the downward motions have larger amplitudes than the upward motions. Near the disk center (Figures 3(a, c)) the correlation is best shown between Hα and C IV redshifts and corresponds to bright

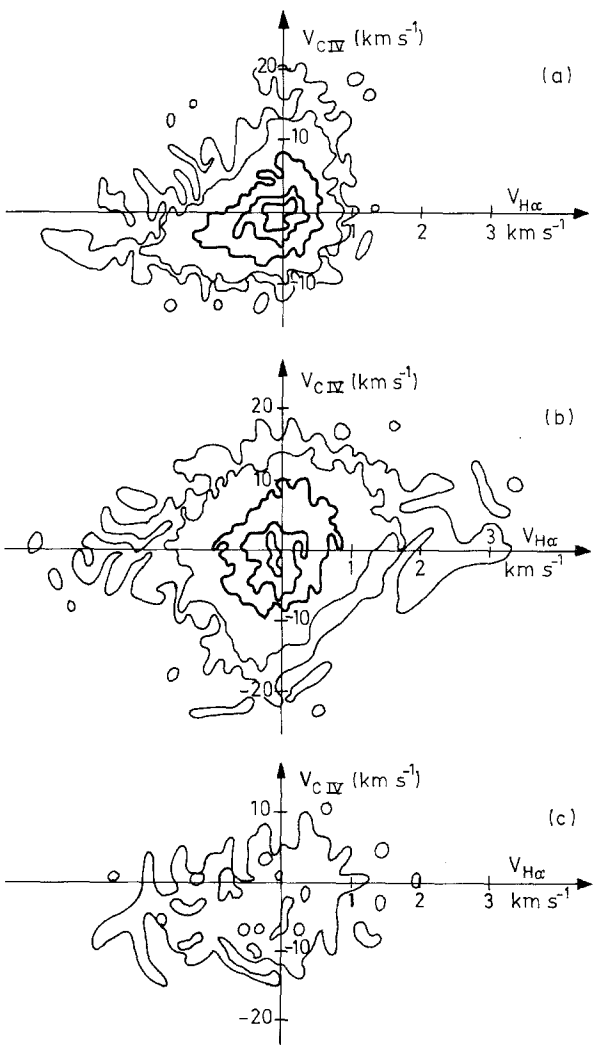

Fig. 3. Histograms of $V_{C\,IV}/V_{H\alpha}$: (a) at the disk center – 2 October, 1980 – on area 4′ × 4′; (b) at the limb – 1 May, 1980 – on area 4′ × 4′; (c) on faculae at the disk center – 2 October, 1980.

regions, as reported in Section 2.2. This is confirmed by the study of faculae (Figure 3(c)).

(2) The region is near the limb (1 May, 1980) (Figure 3(b)). Hα Doppler shift values have a symmetric distribution versus the origin. The horizontal velocities (blue and red shifted) have comparable amplitude maxima. A correlation exists between Hα and C IV blue shifted horizontal velocities.

3.3. Velocity ratio, in faculae and outside

The velocity standard deviations are calculated in 9 Hα velocity fields overlaying partly 21 C IV velocity fields (4′ × 4′) (Table I, Figures 4 and 8(a)) and in selected faculae in these fields of view (Table II, Figures 4 and 8(b)).

In Figure 4, we present the velocity standard deviations calculated over the full field and over faculae, versus the distance r from the disk canter. These values increase with increasing r at chromospheric levels but remain approximately constant in the transition region. It is in good agreement with results of Dere *et al.* (1982) and is compatible with measurements made by Klimchuk (1986) if we take into account the error bars.

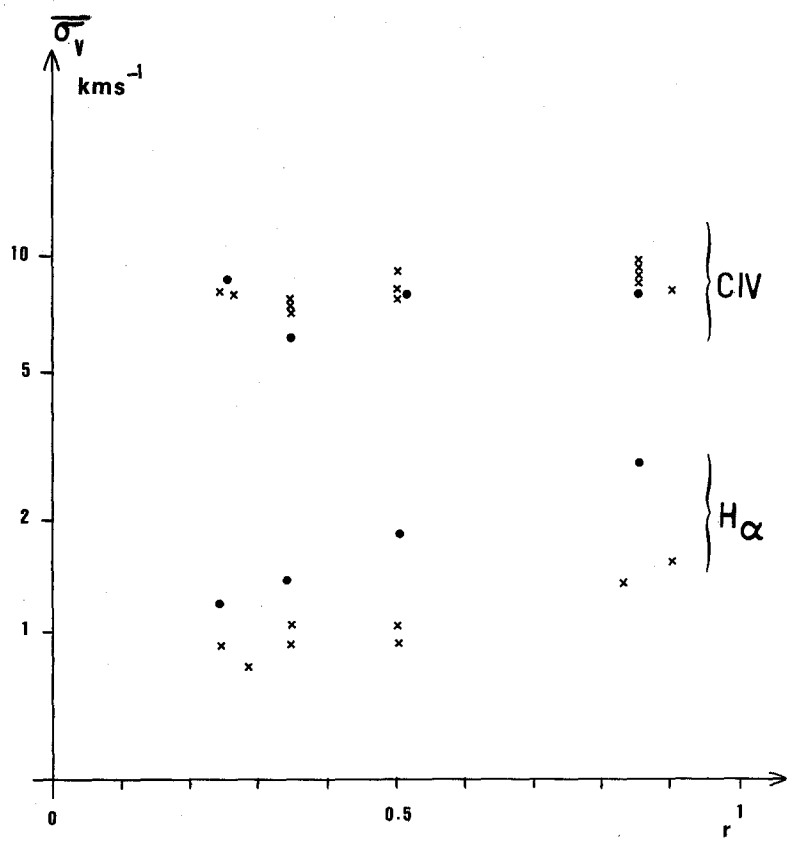

Fig. 4. $\bar{\sigma}_{v\lambda}$ versus the distance to the Sun center r. Crosses refer to values corresponding to the largest field of view superposable in the both lines; circles refer to faculae.

The important point of our present study is the determination of the values of the ratio r_c between Hα and C IV line velocities:

- at the disk center

$$r_c \sim 9, \quad \text{in faculae } r_c^* \sim 7 ;$$

- at the limb

$$r_c \sim 5, \quad \text{in faculae } r_c^* \sim 3 .$$

These results are in good agreement with previous result (Mein *et al.*, 1982). In Section 5 we will use the ratio calculated at the disk center to determine the behaviour of the magnetic field lines, in Section 6 we will discuss the accuracy of these values.

4. Density Model and Geometrical Configuration

4.1. Height of formation of Hα at the disk center

Hα is formed over a wide range of altitudes (Zelenka, 1975). We determine empirically the formation height $z_{1,0}$ relative to velocities by using the observed phase shifts between velocities measured in the Ca II, IR- and K-lines, and in the Hα line. By mean of weighting functions, theoretical formation heights have been calculated for Doppler shifts in Ca II 8542 Å and Ca II 3933 Å (Mein and Mein, 1980). In the case of low frequency waves (valid for stationary motions), they are about 1300 and 1750 km, respectively, in the framework of the HSRA model (Gingerich *et al.*, 1971). Moreover, simultaneous observations of oscillations (Mein and Mein, 1976, p. 242) provided phase shifts between Ca II 8542 Å and Hα and phase shifts between Hα and Ca II 3933 Å, in the case of 3 min periods, when Hα Doppler shifts are measured at the distance ± 0.3 Å from line centre. The ratios of the phase shifts lies between 0.5 and 2, according to the location in the network. We can deduce that the Hα formation height for velocities, is approximately 1500 ± 100 km above $\tau_{5000} = 1$.

In the HSRA atmosphere, this height corresponds to low-hydrogen ionization ($T \sim 7000$ K, $b_1 \sim 20$) and to densities around $\rho(z_{1,0}) = 5 \times 10^{11}$ cm^{-3}. In the model VAL C (quiet Sun), as well as in the VAL E (bright network) (Vernazza *et al.*, 1981), such densities correspond to slightly lower temperatures. However, we can assume that the density scale height and the ionization are not very different. We conclude that computation of formation heights in VAL C or VAL E should lead to similar values of the corresponding density.

4.2. Density model

For the line formation, we use a very simple one-dimensional model.

At the disk center we call $z_{1,0}$ the formation height of radial velocities in Hα, and $\rho_{1,0}$ the corresponding density. At the distance r from the disk-centre, we derive the new Hα-formation height by assuming that the absorption coefficient is proportional to the local density. If we call $H_\rho (\sim 250$ km) a typical chromospheric density scale height, we

get, respectively,

$$z_1 = z_{1,0} - H_\rho \log \sqrt{1 - r^2} \quad \text{and} \quad \rho_1 = \rho_{1,0} \exp((z - z_{1,0})/H_\rho),$$

for the formation height and the corresponding density ($\log \sqrt{1 - r^2} < 0$). The C IV line, almost optically thin, is assumed to be formed at the same height z_2 whatever is the center-to-limb location. The corresponding density is noted ρ_2.

In order to derive the velocities from the assumption of material frozen inside the magnetic flux tubes, we need the density at the Hα and C IV level.

4.3. Determination of $\rho_{1,0}$ and ρ_2 in faculae and in non-facular regions

We have already mentioned that the same value $\rho_{1,0} = 5 \times 10^{11}$ cm^{-3} was acceptable for Hα in faculae and outside. The accuracy of the ratio $\rho_{1,0}/\rho_2$ is clearly limited by the accuracy of ρ_2. Indeed, in the transition region (10^5 K), the dispersion of the C IV density values is large. Dumont *et al.* (1983) give the lowest values, in the faculae $\rho_2^* = 3 \times 10^{10}$ cm^{-3}, in the quiet Sun $\rho_2 = 3 \times 10^9$ cm^{-3}. According to other authors (Feldman *et al.*, 1976; Dupree *et al.*, 1973; Dere *et al.*, 1982), the density can reach higher values $\rho_2^* = 10^{11}$ cm^{-3} in the facular regions and $\rho_2 = 10^{10}$ cm^{-3} in the quiet Sun. These discrepancies between the authors are systematic. But in any case the ratio ρ_2^*/ρ_2 is kept around 10 in the studies where the two different solar regions are compared.

4.4. Ratio of densities $\rho_{1,0}/\rho_2$

According to the preceding results the ratio of densities are $\rho_{1,0}/\rho_2 = 250$ or 50 outside faculae and $\rho_{1,0}^*/\rho_2^* = 15$ or 5 in faculae. These values will be used in Sections 4 and 5. We shall discuss in Section 6 consequences of possible errors in the density ratios.

4.5. Constraints on the geometrical configuration in facular and non-facular regions

At the disk center, the mass flux through a horizontal s is equal to

$$F(s) = \int_0^s \rho V \, \mathrm{d}s,$$

where ρ is the density and V the vertical velocity.

The ratio R of the fluxes observed in the Hα and C IV lines is proportional to

$$R = \frac{F_{\mathrm{C\,IV}}}{F_{\mathrm{H}\alpha}} = r_c \rho_2/\rho_{1,0}.$$

In faculae the ratio is equal to

$$R^* = r_c^* \rho_2^*/\rho_{1,0}^* \quad \text{and} \quad 0.5 \leq R^* \leq 1.4,$$

and outside faculae

$$R = r_c \rho_2 / \rho_{1,0} \quad \text{and} \quad 0.04 \leq R \leq 0.02 .$$

These results indicate that the mass flux is not conserved, except in faculae with some assumption. In quiet regions, the flux tubes corresponding to chromospheric temperature (Hα) may be curved and mostly reconnected below the transition region as suggested by Mein *et al.* (1982). This reconnection could explain the low value of the correlation between Hα and C IV measurements (0.3–0.4).

The horizontal velocities are relatively more important in Hα than in C IV, which suggests a difference between the curvature of the field lines, i.e., less inclined in the chromosphere than in the transition region. Such constraints lead to elaborate models of magnetic field support. The difference of R values in faculae and non facular region can be taken into account by different height scales of the magnetic field ($R^*/R \approx 10$).

5. Order-of-Magnitude Model of Faculae and Non-Facular Regions

The simplest magnetic field model for a periodic arcade is given by:

$$\begin{aligned} B_x &= -B_0 \cos(kx)\, e^{-lz}, \\ B_y &= 0, \\ B_z &= B_0 \sin(kx)\, e^{-lz}, \end{aligned} \tag{1}$$

where z is the vertical coordinate and x and y are tangent to the solar surface. k and l are related, respectively, to the half-width W of the arcade and the magnetic scale height H by

$$k = \pi/2W, \qquad l = \pi/2H . \tag{2}$$

It must be noticed that this magnetic field is potential (current-free) only in the case when $k = l$ ($W = H$).

We are interested in two different cases: the magnetic field above faculae which may be described by the case $k = l$, and the non-facular type magnetic field which may be given by the case $l \gg k (W \gg H)$.

Figure 5 (top) represents a typical potential field for faculae ($k = l$ or $W = H$) and Figure 5 (bottom) shows a flat magnetic configuration that we suggest for non-facular regions ($k = 0.035\, l$ or $H = 0.035$ W). In both cases, the model refers to large-scale lines connecting opposite polarity regions.

The magnitude of the field, $|B| = B_0\, e^{-lz}$, is independent of x. Hence, B_0 is the magnitude of the field at the base.

5.1. A STATIC ORDER-OF-MAGNITUDE MODEL

In the case of the potential facular type field ($k = l$), the momentum equation reduces to

$$\frac{\partial P}{\partial z} = -\rho g \tag{3}$$

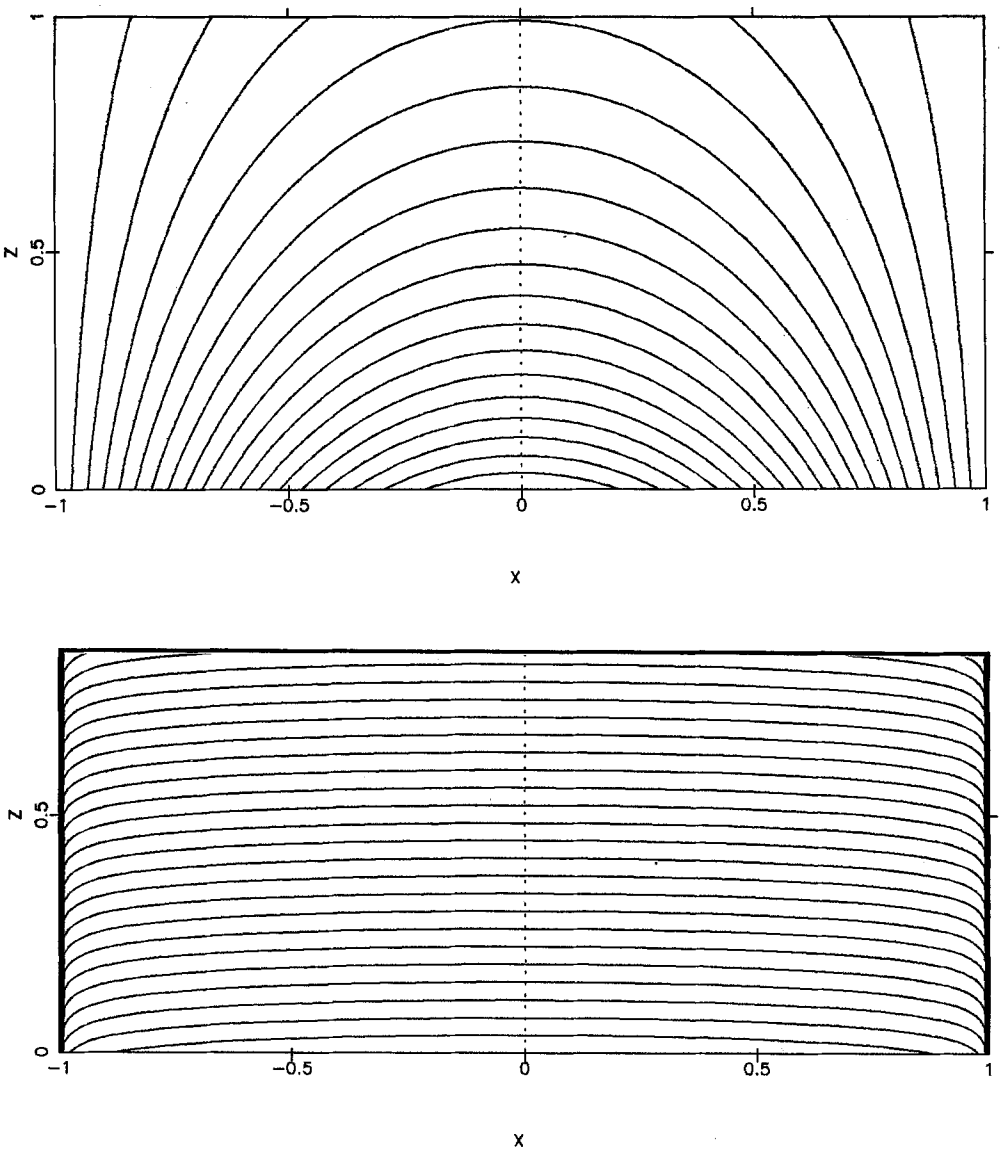

Fig. 5. *Top*: magnetic field lines with $H = W$; *bottom*: magnetic field lines with $H = 0.035W$.

and the density distribution with height is independent of the field (P, ρ, g have their usual meaning).

In the non-facular type magnetic configuration ($k \gg l$), the momentum equations are

$$\frac{\partial P}{\partial x} = f_x\,, \qquad (4)$$

$$\frac{\partial P}{\partial z} = f_z - \rho g\,,$$

where $\mathbf{f} = (f_x, 0, f_z)$ is the Lorentz force $(\mathbf{j} \wedge \mathbf{B})$ and $\mathbf{j}$ is the current density. The Lorentz force is given by

$$\mathbf{f} = \frac{B_0^2}{\mu_0} e^{-2lz}(l - k)\cos(kx)\,[\sin(kx), 0, \cos(kx)] \tag{5}$$

and is orthogonal to the field lines. Its magnitude is given by

$$f = \frac{B_0^2}{\mu_0} e^{-2lz}(l - k)\cos(kx)\,. \tag{6}$$

This force is directed outwards when $l > k$ (non-facular regions) $(W > H)$ or inwards when $l < k (W = H)$, hence, it tends to open the non-facular type magnetic field. To balance this force, the density must not decrease so fast with height, as it does in the case when the atmosphere is magnetically force-free. We now try to investigate what implies, on the density distribution, the presence of the above magnetic force.

Let us assume that the atmosphere is isothermal, and look at the equilibrium of the top of the arcade.

This equilibrium $(x = 0)$ is governed by

$$\begin{aligned} &\frac{\partial P}{\partial z} = -\rho g + \frac{B_0^2}{\mu_0} e^{-2lz}(l - k)\,, \\ &P = \rho kT/m \end{aligned} \tag{7}$$

(k = Boltzmann constant, m = mean molecular mass).

We now introduce the pressure scale height $D = kT/gm$ and the plasma β defined by $\beta = P_0/(B_0^2/2\mu_0)$, with subscript 0 referring to the base $(z = 0)$. Introducing the non-dimensional quantities $\bar{\rho} = \rho/\rho_0$ and $\bar{z} = z/D$, we write the equilibrium equation in the form

$$\frac{\partial \bar{\rho}}{\partial \bar{z}} = -\bar{\rho} + \frac{2}{\beta}(l - k)D\, e^{-2lD\bar{z}}\,. \tag{8}$$

Integrating this equation from $\bar{z} = 0$ and $\bar{\rho} = 1$, we obtain

$$\bar{\rho} = e^{-\bar{z}} + \frac{2}{\beta}\frac{(l - k)D}{1 - 2lD}(e^{-2lD\bar{z}} - e^{-\bar{z}}) = \bar{\rho}_1 + \bar{\rho}_2\,. \tag{9}$$

The first term $\bar{\rho}_1$ is the well-known isothermal law for a force-free or current-free or non-magnetized atmosphere, while the second term $\bar{\rho}_2$ is due to the presence of non-force-free magnetic field. It is interesting to examine the behaviour of the ratio $\bar{\rho}/\bar{\rho}_1$:

$$\frac{\bar{\rho}}{\bar{\rho}_1} = 1 + \frac{2}{\beta}\frac{(l - k)D}{1 - 2lD}(e^{\bar{z}(1-2lD)} - 1)\,. \tag{10}$$

In the case when $l > k (W > H)$, this equation always satisfies the inequality

$$\bar{\rho}/\bar{\rho}_1 > 1 .$$

This means that a larger amount of material must be available to adjust equilibrium in the presence of a non-force-free magnetic field.

For a non-facular type field ($l \gg k$) or $W \gg H$, at coronal or transition region temperatures, we have $lD \gg 1$. Hence, for reasonable altitudes, the ratio $\bar{\rho}/\bar{\rho}_1$ becomes $\bar{\rho}/\bar{\rho}_1\ 1 + 1/\beta$, and may be greater than 10 in the transition region (with $\beta < 0.1$), or 100 in the corona (with $\beta < 0.01$).

At chromospheric temperatures (Hα line for instance) we have $lD \approx 1$ ($D \approx H$). Hence, the ratio $\bar{\rho}/\bar{\rho}_1$ is given by

$$\frac{\bar{\rho}}{\bar{\rho}_1} \approx 1 + \frac{2}{\beta} lD\bar{z} \tag{11}$$

and is greater than one, but smaller than, say, 5 (with $\beta \approx 1$).

These results show that the ratio $\bar{\rho}/\bar{\rho}_1$ and, hence, the difference between the classical atmosphere with force-free field and the atmosphere with non-force-free field depends essentially on the plasma β.

This difference is small at low temperatures (chromosphere and transition region), but important in the corona.

In the presence of the non-force-free magnetic fields, the density does not decrease so fast as in the case with force-free field. At large distances in an isothermal corona, the density varies as

$$\bar{\rho} = e^{-\bar{z}} \left(1 + \frac{1}{\beta}\right)$$

instead of

$$\bar{\rho} = e^{-\bar{z}} .$$

5.2. A DYNAMIC ORDER-OF-MAGNITUDE MODEL

In the following, instead of solving the full set of hydrodynamic equations, we simply use mass continuity for a steady flow and magnetic flux conservation which can be written, along a magnetic tube, as

$$\frac{\rho v}{B} = \frac{\rho_0 v_0}{B_0} = \text{constant} , \tag{12}$$

where ρ, v, B have their usual meaning.

We now assume that:

- the velocity at the base of the structure ($z = 0$) is constant everywhere;
- the density is a function of z only (plan parallel atmosphere); we do not formulate

any assumption on the temperature, and do not solve the momentum equation. We do not try to solve the force balance equations in the non-force-free case. Consequently, the results of the model developed in Section 5.1 are not valid for this dynamic model, which is consistent with a continuous rise of the magnetic lines.

As the magnetic field strength B is a function of z only (see Section 5.1) we obtain

$$\frac{\rho(z)v(z)}{B(z)} = \frac{\rho_0 v_0}{B_0} = \text{constant}\,.$$

We also assume that the formation heights for C IV and Hα lines are z_1 and z_2, respectively (Figure 6), and, using the coordinate system of Figure 6, we get

$$\begin{aligned} V_{\mathrm{C\,IV}}(x) &= \frac{\rho_0 v_0}{B_0 \rho(z_2)} [B_z(x, z_2)\cos\theta + B_x(x, z_2)\sin\theta\sin\varphi]\,, \\ V_{\mathrm{H}\alpha}(x) &= \frac{\rho_0 v_0}{B_0 \rho(z_1)} [B_z(x - \mathrm{tg}\,\theta\sin\varphi\,\Delta z, z_1)\cos\theta + \\ &\quad + B_x(x - \mathrm{tg}\,\theta\sin\varphi\,\Delta z, z_1)\sin\theta\sin\varphi]\,, \end{aligned} \tag{13}$$

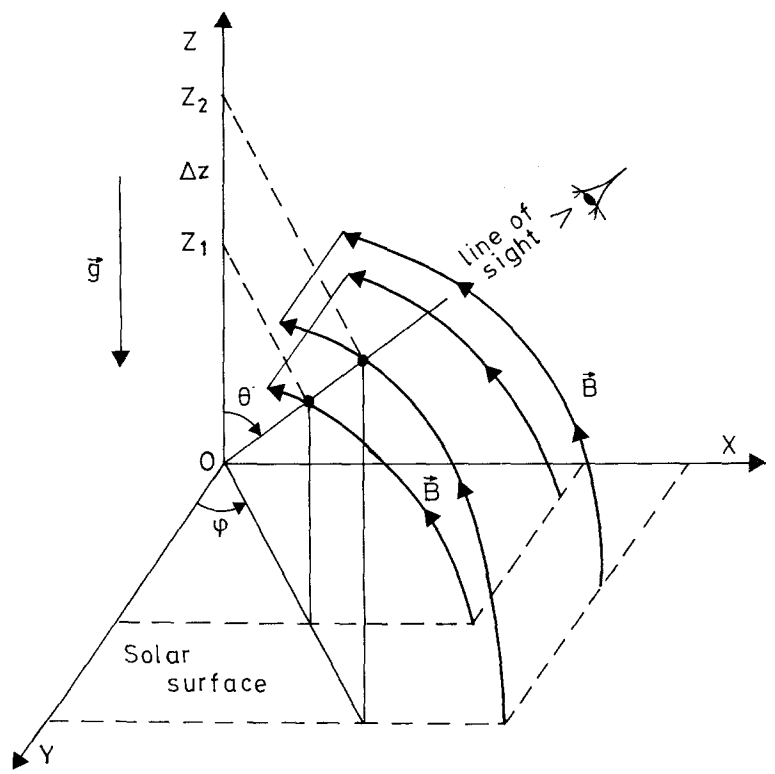

Fig. 6. The coordinate system used in the paper. The plane $(x, 0, y)$ is tangent to the solar surface and the z-axis is vertical (opposite to gravity). The line-of-sight is defined by angles θ $(0 \le \theta \le \pi/2)$ and $\varphi(-\frac{1}{2}\pi \le \varphi \le \frac{1}{2}\pi)$. The field lines have a symmetry of translation along the y-direction. $z_{1,0}$ and z_2 are the formation heights for Hα and the C IV line, respectively.

where $V_{\mathrm{C\,IV}}$ and $V_{\mathrm{H}\alpha}$ are line-of-sight velocities, and $\Delta z = z_2 - z_1$. We normalize quantities to the base values, such as

$$\overline{V} = V/V_0\,, \qquad \overline{\rho} = \rho/\rho_0\,, \qquad \overline{B} = B/B_0\,, \tag{14}$$

and obtain

$$\begin{aligned}
\overline{V}_{\mathrm{C\,IV}}(\theta, \varphi, x) &= \frac{1}{\overline{\rho}(z_2)}\,[\overline{B}_z(x, z_2)\cos\theta + \overline{B}_x(x, z_2)\sin\theta\sin\varphi]\,, \\
\overline{V}_{\mathrm{H}\alpha}(\theta, \varphi, x) &= \frac{1}{\overline{\rho}(z_1)}\,[\overline{B}_x(x - \mathrm{tg}\,\theta\sin\varphi\,\Delta z, z_1)\cos\theta + \\
&\quad + \overline{B}_x(x - \mathrm{tg}\,\theta\sin\varphi\,\Delta z, z_1)\sin\theta\sin\varphi]\,.
\end{aligned} \tag{15}$$

We use for C IV a constant formation height (z_2). For Hα, we use the density model of Section 4.2, so that

$$z_1 = z_{1,0} - H_\rho \log\sqrt{1 - r^2}$$

and

$$\overline{\rho}(z_1) = \overline{\rho}(z_{1,0})\exp[(z_1 - z_{1,0})/H_\rho]\,,$$

H_ρ being a typical pressure scale height, and $r = \sin\theta$ being the angular distance between the normal to the solar surface and the line-of-sight.

As the angle φ is an unknown quantity which may take arbitrary values in the range $[-\pi/2$ to $\pi/2]$, we integrate over φ and get the average velocity:

$$\overline{V}_{A,\lambda}(x, r) = \frac{1}{\pi}\int_{-\pi/2}^{\pi/2} \overline{V}_\lambda(\theta, \varphi, x)\,\mathrm{d}\varphi\,. \tag{16}$$

We also integrate over x in the range $(-W, W)$ and get the r.m.s. velocity:

$$\overline{V}_{B,\lambda}(v) = \frac{1}{2\pi W}\int_{-\pi/2}^{\pi/2}\left[\int_{-W}^{W} \overline{V}_\lambda^2(\theta, \varphi, x)\,\mathrm{d}x\right]^{1/2} d\varphi\,, \tag{17}$$

where $r = \sin\theta$ and $\lambda =$ C IV or Hα. $\overline{V}_A$ is the mean velocity and $\overline{V}_B$ the root mean square velocity along the line-of-sight. Both are observationnaly measured (see previous sections and Figures 3 and 4). Figure 7 shows theoretical histograms of C IV velocity ($\overline{V}_{A,\,\mathrm{C\,IV}}$) versus H$\alpha$ velocity ($\overline{V}_{A,\,\mathrm{H}\alpha}$) for different values of r. A good correlation is found between velocities computed at these different levels and a good agreement is obtained between observational (Figure 3) and theoretical (Figure 7) data. For the calculations, we took $-W < x < W$, $z_2/W = 0.2$, $z_{1,0}/W = 0.15 = z_1(r = 0)/W$, assuming the following values for $z_{1,0}$, z_2, and W: $z_{1,0} = 1500$ km; $z_2 = 2000$ km and $W = 10\,000$ km. $2W$ is the typical size of network cells or the distance between opposite polarity faculae.

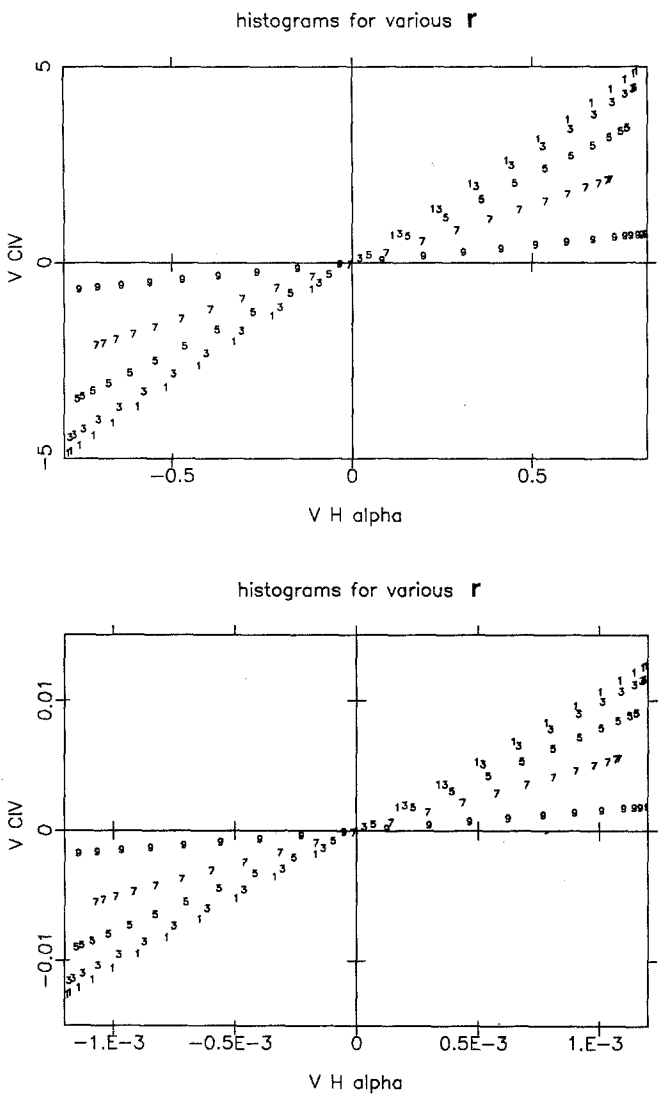

Fig. 7. Theoretical histograms of C IV and Hα radial velocities for various $r = \sin\theta$ values. The velocities may be multiplied by an arbitrary factor (the base velocity). Curves: 1: $r = 0$ ($\theta = 0°$); 3: $r = 0.4$ ($\theta = 23.6°$); 5: $r = 0.7$ ($\theta = 44.4°$); 7: $r = 0.9$ ($\theta = 64.2°$); 9: $r = 0.99$ ($\theta = 81.2°$). *Top*: $H = W$; $\rho_{H\alpha}/\rho_{C\,IV}$ ($r = 0$) = 6.67; *bottom*: $H = 0.035W$; $\rho_{H\alpha}/\rho_{C\,IV}$ ($r = 0$) = 100.

Figure 7 (top) exhibits results obtained with $\rho_{H\alpha}(r = 0)/\rho_{C\,IV} = \rho(z_{1,0})/\rho(z_2) = 6.67$, $H/W = 1$ (potential field), and Figure 7 (bottom) shows results obtained with $\rho_{H\alpha}/\rho_{C\,IV}(r = 0) = \rho(z_{1,0})/\rho(z_2) = 100$, $H/W = 0.035$ (non-force-free field).

In these calculations, the pressure scale height for the Hα density model was $D/W = 0.025$ (assuming that $D = 250$ km if $W = 10\,000$ km).

Figure 8 (top) shows plots of $\overline{V}_{B,\,C\,IV}(r)$ and $\overline{V}_{B,\,H\alpha}(r)$ as functions of r(0 = disk centre, 1 = limb), with $\rho_{H\alpha}(r = 0)/\rho_{C\,IV} = \rho(z_{1,0})/\rho(z_2) = 6.67$, and $H/W = 1$, while Figure 8

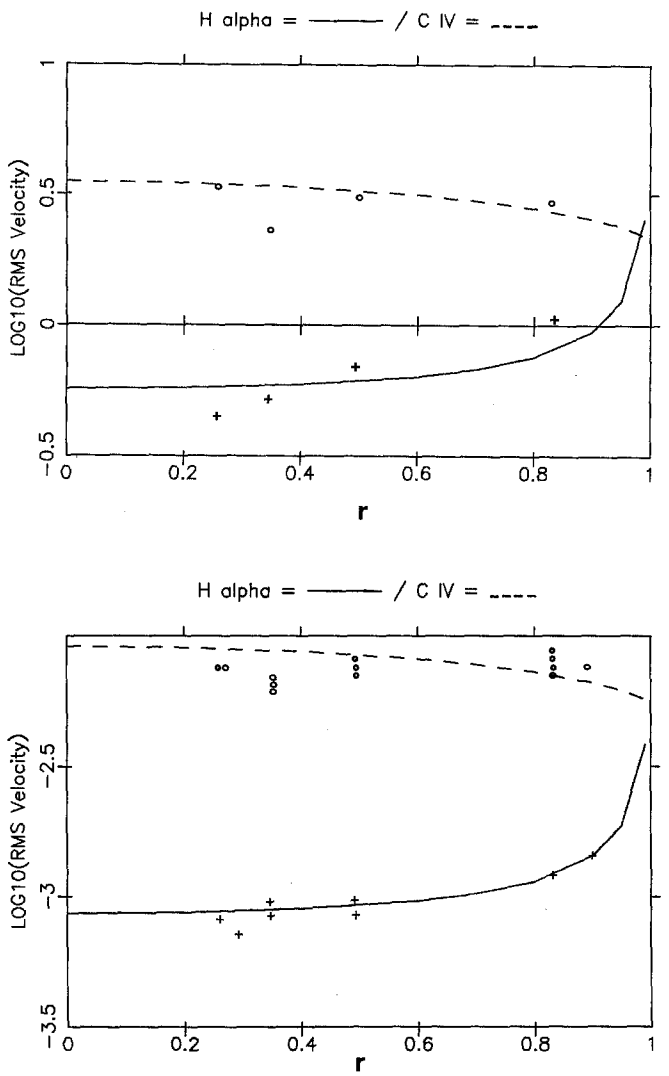

Fig. 8. Theoretical variation of C IV (dashed line) and Hα (continuous line) radial r.m.s. velocities as functions of $r = \sin\theta$. Crosses (+) represent observed Hα values, while circles (○) indicate C IV measurements. *Top*: $H = W$; $\rho_{H\alpha}/\rho_{C\,IV}\,(r = 0) = 6.67$ (potential field). Facula data are reported. *Bottom*: $H = 0.035W$; $\rho_{H\alpha}/\rho_{C\,IV}\,(r = 0) = 100$ (non-force-free field). Non-facular regions data (the whole field of view, except the faculae) are displayed. The theoretical velocities are shown *in logarithmic scale* and may be multiplied by an arbitrary factor (the base velocity); so the fitting between observational and computed values was performed by translating observed data upon calculated ones.

(bottom) shows results obtained for the case $\rho_{H\alpha}(r = 0)/\rho_{C\,IV} = \rho(z_{1,0})/\rho(z_2) = 100$, and $H/W = 0.035$. Observational measurements (top: faculae and bottom: non-facular regions) are shown in these figures and are in good agreement with computed values.

6. Discussion

The models described in Section 5 are fully characterized by the ratio between vertical and horizontal H/W scales of magnetic loops. This ratio was connected with the ratio of the mean quadratic radial mass fluxes $\rho_2 V_2/\rho_{1,0} V_{1,0}$ observed at two different altitudes. Figure 8 shows that the center-to-limb behaviour, strongly related to the opacity in the lines under study (Hα or C IV), was qualitatively in agreement with the curves predicted theoretically. The discussion concerning the fit of the models with the centre-disk values is more crucial. We have to look now into the possible influence of errors on assumed densities and velocity ratios as well as into possible effects of oscillations.

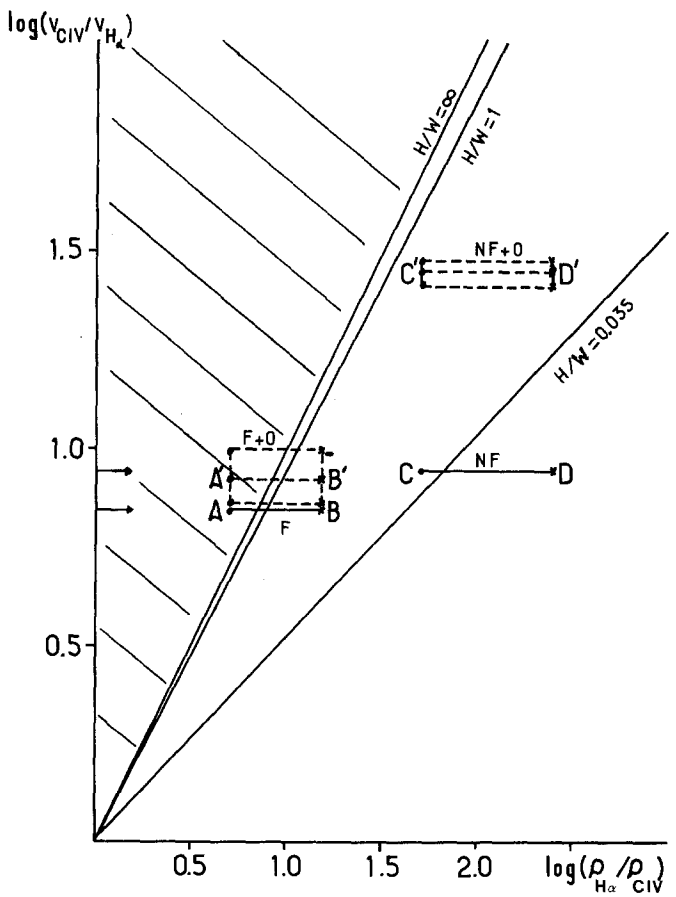

Fig. 9. Diagram velocity ratio at the disk center versus density ratio between Hα and C IV lines. Crosses indicate Dumont *et al.* density values, dots other author values in the transition zone – in the facular (F) and non-facular regions (NF), the horizontal straight lines indicate the density error bars and our velocity ratio results; the dashed horizontal ones, the values corrected by the oscillations of 5 min, with the error bars. The error bars for velocity ratios (order of magnitude 0.05; see Section 6) are not drawn; H/W is the ratio between the horizontal and the vertical height scales in the magnetic models used in the two regions (F and NF). The hatched region corresponds to open structures.

Density values at both levels $\rho_{1,0}$ and ρ_2 are linked to our models through their ratio $\rho_{1,0}/\rho_2 = \rho_{H\alpha}/\rho_{C\,IV}$. In the plane $(\rho_{H\alpha}/\rho_{C\,IV})$, $(V_{C\,IV}/V_{H\alpha})$, density models are represented by vertical lines, and magnetic models by straight lines intersecting at the origin (Figure 9). The dashed region correspond to mean fluxes larger at high altitude than at low altitudes, which is an irrelevant situation for magnetic loopd rooted in lower levels. We have plotted the velocity ratios observed in this work at disk-centre (7 and 9 km s^{-1}, respectively). In the magnetic model calculation, the formation heights of velocities has been assumed to be respectively 1500 and 2000 km, and the horizontal half-width of the arcades equal to 10000 km. The horizontal error bars show the range of density models given by various authors. We see that *all possible values H/W* are *larger for facular regions* (F) than for non-facular regions (NF).

The error on the ratio of the velocities is dominated by the uncertainty on the value of the mean velocity for the C IV line, as pointed to in Section 2.2. For instance, a systematic error of 4 km s^{-1} will change the r.m.s. velocity from 8 km s^{-1} to approximately 9 km s^{-1}, which corresponds to a relative error of 0.12 on the ratio r_c.

Figure 9 shows also what happens if we take into account the 3 (or 5) mn-oscillations of velocity. Their contribution to radial velocities is negligible for the C IV line (Malherbe *et al.*, 1987), for Hα line it can be estimated to $\frac{1}{3}$ in the chromospheric bright regions and $\frac{9}{10}$ in the quiet Sun from velocity power spectrum study with an uncertainty of 15% (Mein and Mein, 1976, p. 237). As a consequence, $V_{C\,IV}/V_{H\alpha}$ is increased, as well as the corresponding value H/W defining the magnetic models (8.6 in F – 28 in NF). We see immediately that the effect will be qualitatively significant only if the new H/W-value for non-facular regions exceeds the lowest possible one for faculae.

This can only occur in a small region near C', but this solution has to be eliminated of we keep the ratio $\rho_2^*/\rho_2 = 10$ (see Section 4.3).

In conclusion, the magnetic loops close definitely at higher levels above faculae than above non-facular regions.

7. Conclusion

Using simultaneous observations of the same solar region in the lines Hα and C IV 1548 Å, we have derived schematic models of closed magnetic lines from dynamical constraints. We have assumed that mean fluxes were flowing along magnetic lines, which is probably a very good approximation. But we had to do also more questionable assumptions: closed loops rooted in the photosphere, stationary magnetic and velocity fields, neglected systematic mean flow in the whole observed region. In this context we have concluded that:

– the shape of magnetic loops is different above facular and non-facular regions (H/W higher and loops closed at higher levels in the first case);

– this result remains valid, whatever are the assumed density models, and even if we take into account the 3 mn oscillations;

– the center-to-limb behaviour is well predicted by taking into account the relative opacity in chromosphere and transition region.

We think that such an approach of magnetic line geometry can be helpful in the general problem of canopy-type configuration.

Acknowledgements

We would like to thank Dr S. Dumont for helpful discussions and comments about this paper, and also C. Coutard, R. Hellier, and A. Miguel for the quality of Hα data obtained with MSDP of the Meudon Solar Tower. Space Ooservations were made possible by the assistance of UVSP/SMM Staff (NASA Guest Investigator Program on SMM). We also thank C. Bréchet and I. Baroux for their help in reducing the data, and S. Bordet for typing the manuscript. Computations were performed on the VAX at the Observatory of Meudon.

References

Athay, R. G., Gurman, J. B., Henze, W., and Shine, R. A.: 1983, *Astrophys. J.* **265**, 519.
Athay, R. G. and White, O. R.: 1978, *Astrophys. J.* **220**, 1135.
Brueckner, G. E.: 1981, in F. Orrall (ed.), *Monograph from Skylab Solar Workshop III*, p. 113.
Dere, K. P.: 1981, *Solar Phys.* **75**, 189.
Dere, K. P., Bartoe, J. D. F., and Brueckner, G. E.: 1982, *Bull. Am. Astron. Soc.* **13**, 845.
Deubner, F. L.: 1975, *Astron. Astrophys.* **44**, 371.
Doschek, G. A., Feldman, U., and Bohlin, J. D.: 1976, *Astrophys. J.* **205**, L117.
Dumont, S., Mouradian, Z., Pecker, J. C., Vial, J. C., and Chipman, E.: 1983, *Solar Phys.* **83**, 27.
Dupree, A. K., Huber, M. C. E., Noyes, R. W., Parkinson, W. H., Reeves, E. M., and Withbroe, G. I.: 1973, *Astrophys. J.* **182**, 321.
Evans, J. W. and Michard, R.: 1962, *Astrophys. J.* **136**, 493.
Feldman, V., Doschek, G. A., and Patterson, N. P.: 1976, *Astrophys. J.* **209**, 270.
Gebbie, K. B., Hill, F., Tomre, J., November, L. J., Simon, G. W., Gurman, J. B., Shine, R. A., Woodgate, B. E., Athay, R. G., Bruner, E. L., and Rehse, R. A.: 1981, *Astrophys. J.* **251**, L115.
Gingerich, O., Noyes, R. W., and Kalkofen, N.: 1971, *Solar Phys.* **18**, 347.
Giovanelli, R. G. and Jones, J. P.: 1982, *Solar Phys.* **79**, 267.
Jones, H. P. and Giovanelli, R. G.: 1982, *Solar Phys.* **79**, 247.
Klimchuk, J. A.: 1986, Thesis, NCAR, University of Colorado.
Melherbe, J. M., Schmieder, B., Ribes, E., and Mein, P.: 1983, *Astron. Astrophys.* **119**, 197.
Malherbe, J. M., Schmieder, B., Mein, P., and Tandberg-Hansen, E. A.: 1987, *Astron. Astrophys.* **174**, 316.
Mariska, J. T.: 1986, *Ann. Rev. Astron. Astrophys.* **24**, 23.
Mein, P.: 1977, *Solar Phys.* **54**, 45.
Mein, N. and Schmieder, B.: 1981, *Astron. Astrophys.* **97**, 310.
Mein, N. and Provost, J.: 1979, *Solar Phys.* **3**, 367.
Mein, N. and Mein, P.: 1976, *Solar Phys.* **49**, 231.
Mein, N. and Mein, P.: 1980, *Astron. Astrophys.* **84**, 96.
Mein, P., Simon, G., Vial, J. C., and Shine, R. A.: 1982, *Astron. Astrophys.* **111**, 136.
Roussel-Dupré, D. C. and Shine, R. A.: 1982, *Solar Phys.* **77**, 329.
Schmieder, B., Malherbe, J. M., Mein, P., and Tandberg-Hansen, E. A.: 1984a, *Astron. Astrophys.* **94**, 133.
Schmieder, B., Mein, P., Martres, M. J., and Tandberg-Hanssen, E. A.: 1984b, *Solar Phys.* **136**, 81.
Simon, G., Mein, P., Vial, J. C., Shine, R. A., and Woodgate, B. E.: 1982, *Astron. Astrophys.* **115**, 367.
Tandberg-Hanssen, E. A.: 1981, *Astrophys. J.* **251**, L115.
Vernazza, J. E., Avrett, E. H., and Loeser, R.: 1981, *Astrophys. J., Suppl.* **4**, No. 4.
Withbroe, G. L. and Noyes, R. W.: 1977, *Ann. Rev. Astron. Astrophys.* **15**, 363.
Woodgate, B. E., Tandberg-Hanssen, E. A., Bruner, E. C., Beckers, J. M., Brandt, J. C., Henze, W., Hyder, C. L., Kalet, M. W., Kenny, P. J., Knox, E. D., Michialitsianos, A. G., Rehse, R., Shine, R. A., and Tinsley, H. D.: 1980, *Solar Phys.* **65**, 73.
Zelenka, A.: 1975, *Solar Phys.* **40**, 39.